Chemical Science

ROYAL SOCIETY OF CHEMISTRY

EDGE ARTICLE

View Article Online
View Journal | View Issue

Cite this: *Chem. Sci.*, 2023, **14**, 11456

All publication charges for this article have been paid for by the Royal Society of Chemistry

Regulating the orientation of a single coordinate bond by the synergistic action of mechanical forces and electric field†

Wei Zhang,[a] Zhibin Zhao,[a] Min Tan,[a] Adila Adijiang,[a] Shurong Zhong,[a] Xiaona Xu,[a] Tianran Zhao,[a] Emusani Ramya,[a] Lu Sun,[a] Xueyan Zhao,[a] Zhiqiang Fan *[b] and Dong Xiang *[ac]

Received 27th July 2023
Accepted 30th September 2023

DOI: 10.1039/d3sc03892k

rsc.li/chemical-science

The molecular binding orientation with respect to the electrode plays a pivotal role in determining the performance of molecular devices. However, accomplishing *in situ* modulation of single-molecule binding orientation remains a great challenge due to the lack of suitable testing systems and characterization approaches. To this end, by employing a developed STM-BJ technique, we demonstrate that the conductance of pyridine-anchored molecular junctions decreases as the applied voltage increases, which is determined by the repeated formation of thousands of gold–molecule–gold dynamic break junctions. In contrast, the static fixed molecular junctions (the distance between two electrodes is fixed) with identical molecules exhibit a reverse tendency as the bias voltage increases. Supported by flicker noise measurements and theoretical calculations, we provide compelling evidence that the orientation of nitrogen–gold bonds (a universal coordinate bond) in the pyridine-anchored molecular junctions can be manipulated to align with the electric field by the synergistic action of the mechanical stretching force and the electric fields, whereas either stimulus alone cannot achieve the same effect. Our study provides a framework for characterizing and regulating the orientation of a single coordinate bond, offering an approach to control electron transport through single molecular junctions.

Introduction

Modulation of the electron transport properties through molecular junctions at the single-molecule level is crucial to the development of single-molecule devices.[1–4] Previous reports have proved that molecule conductance can be effectively regulated by external stimuli, such as gating voltage,[5,6] light,[7–9] mechanical force,[10,11] and temperature.[12,13] One impressive feature of the molecular junctions is that the distance between the source and drain electrodes is quite small down to sub-nanometer and thus the electric field can be exceptionally large even when only a small voltage is applied.[14,15] By utilizing the intense electric field, molecules can undergo hydrogen tautomerization,[16] redox reactions,[17] chemical catalysis,[18,19] bond rupture,[20–23] and conductance switching.[24–26] It will be wonderful if we can continuously control *in situ* the single chemical bond orientation by directly controlling the electric field (bias voltage). However, it has barely been reported primarily due to the absence of suitable testing systems and approaches.

Meanwhile, for certain molecules with π-system coupling to electrodes, even a small change in the binding orientation can lead to a substantial alteration in the molecular junction conductance,[27] making them an ideal system for investigating molecular binding orientation. Utilizing these specific molecules, we demonstrated that the orientation of a coordinate bond can be regulated by an external electrical field in a dynamic break junction, but cannot be regulated in a fixed junction. Employing the scanning tunneling microscopy break junction (STM-BJ) technique with a developed electrode suspension function, two types of contrasting molecular break junctions were constructed and the conductance evolution upon increased bias was monitored to quantify the change of bond orientation.[28,29] The first type consists of pyridine-anchored molecular break junctions, where the π-binding can occur between the aromatic ring and electrode, and thus the conductance of the molecular junction is highly sensitive to the bonding orientation of the anchoring group. As the bias voltage increases, a decrease in the conductance of pyridine-anchored molecular junctions was observed by the repeated formation

[a]*Institute of Modern Optics, Center of Single Molecule Sciences, Key Laboratory of Micro-scale Optical Information Science and Technology, Nankai University, Tianjin 300350, China*

[b]*School of Physics and Electronic Science, Changsha University of Science and Technology, Changsha 410114, China*

[c]*School of Materials Science and Engineering, Smart Sensing Interdisciplinary Science Center, Nankai University, Tianjin 300350, China. E-mail: zqfan@csust.edu.cn; xiangdongde@nankai.edu.cn*

† Electronic supplementary information (ESI) available. See DOI: https://doi.org/10.1039/d3sc03892k

and breakage of thousands of single-molecule junctions. The second kind consists of amino-anchored molecular break junctions that are devoid of the π-binding between an aromatic ring and electrode. In line with this, we found that at larger bias voltages, the conductance of amino-anchored molecular break junctions essentially remained unaltered. Assisted by flicker noise measurement and density functional theory (DFT) calculation, it is revealed that the conductance change in the pyridine-anchored molecular junction originates from the alteration of coordinate bond orientation regulated by the synergistic action of electric field and mechanical stretching.

To reveal the role of mechanical stretching in regulating the bonding orientation, we established static fixed junctions by halting the movement of the top electrode once a molecule-bridged junction was formed. In contrast to the behavior demonstrated in the dynamic break junctions, the conductance derived from the *I–V* curves of both the pyridine-anchored and amino-anchored molecular junctions increases as the applied bias voltage increases. These differences indicate that the electric field applied in the experiment alone is insufficient to regulate the orientation of the nitrogen–gold bond. Instead, a synergistic action of mechanical forces and the electric field enables the regulation of coordinate bond orientation.

Results and discussion

Conductance of dynamic molecular break junctions

Fig. 1a illustrates the strategy for the conductance measurement of the 4,4′-di(4-pyridyl)biphenyl (labeled as PY[4]) molecular junction using the STM-BJ technique. All the molecules utilized in the experiments were dissolved in 1,2,4-trichlorobenzene (Aladdin, >99%) with a concentration of 0.5 mmol L^{-1} for electrical characterization. The STM tip for current measurement was prepared by burning one end of a gold wire (250 μm in diameter) with a butane-mixed flame, see ESI Fig. S1 and S2† for detailed information regarding sample preparation. Two types of electrical measurements were performed in the solution environment after the molecules' self-assembling process. One is the conductance measurement based on thousands of dynamic molecule break junctions employing the STM-BJ technique. By controlling the displacement of the STM tip, a molecule-bridged junction can be repeatedly formed *via* the nitrogen–gold link and broken subsequently. Thousands of conductance–displacement traces were recorded during the stretching process, and were used to construct conductance histograms, which determined the probable conductance of the junctions.

Fig. 1b shows typical conductance–displacement traces under different bias voltages. The gray traces show the conductance of a bare gold contact measured in the pure 1,2,4-trichlorobenzene (TCB) solvent. Integer multiples of G_0 ($G_0 = 2e^2/h \approx 77.5$ μS) can be observed with no additional conductance plateau below 1 G_0. In contrast, the conductance plateaus below 1 G_0 were clearly observed when the conductance measurement was performed in PY[4] containing solution. A close examination of the traces reveals that the conductance plateaus shift down as the bias voltage increases. Fig. 1c presents the one-dimensional (1D) conductance histograms of PY[4] molecular junctions at the bias voltages of 100 mV, 200 mV, 300 mV, and 400 mV, respectively. Each of them was constructed from approximately 3000 conductance–displacement traces without data selection. The peak position indicates the probable conductance of the PY[4] molecular junction. As the bias voltage increases from 100 mV to 400 mV, the conductance continuously shifts from 4.5×10^{-5} G_0 (≈3.51 nS) to 8.6×10^{-6} G_0 (≈0.66 nS). The corresponding two-dimensional (2D) conductance histogram is shown in ESI Fig. S3,† which confirms that the conductance of molecular junction decreases as the bias voltage increases. The conductance evolution under negative bias exhibits a similar trend, *i.e.*, the conductance of the molecule junction decreases as the absolute value of the bias increases.

In contrast, for *p*,*p*′-diaminoquaterphenyl (labeled as NH_2[4]) molecules which possess similar backbone structures to PY[4] but different anchoring groups (*i.e.*, amino group) at both ends, the conductance remains almost unchanged when the applied bias voltage changed from 100 mV to 400 mV (Fig. 1d–f), and the corresponding 2D conductance histograms are shown in ESI Fig. S4.† Similarly, the conductance of the NH_2[4] molecule remains constant when the applied negative bias changed from −100 mV to −400 mV. To verify the reliability of the observation that pyridyl-terminated molecules and amino-terminated molecules show discrepant behavior, we investigated a series of molecules with two different anchoring groups, *i.e.*, 1,4-bis(pyrid-4-yl)benzene (labeled PY[3]), 4,4′-bipyridine (labeled as PY[2]), 4,4″-diamino-*p*-terphenyl (labeled as NH_2[3]), and *p*,*p*′-diaminoquaterphenyl (labeled as NH_2[2]), respectively.

Fig. 2a and b show the 1D conductance histograms of PY[3] and PY[2] molecular junctions, respectively. Similar to PY[4], the conductance of PY[3] and PY[2] molecular junctions decreases when the applied bias voltage increases, as demonstrated by the conductance histograms. On close examination of Fig. 2b, additional minor peaks can be seen that are left-shifted as the bias voltage increases and situated at low conductance locations, as indicated by the star symbol. We assign the small peaks to the new type of molecular junctions (*i.e.*, PY[2] dimer formed *via* π–π stacking)[30–32] rather than the varied configuration of single PY[2] junctions upon mechanical stretching, since the low conductance plateau is parallel to the high conductance plateau (*i.e.*, two conductance plateaus appeared simultaneously rather than in sequence), as shown in ESI Fig. S7.† This claim is further supported by the flicker noise measurement which will be explained in more detail later.

In contrast, as illustrated in Fig. 2d and e, the applied bias voltages do not affect the conductance of NH_2[3] and NH_2[2] molecular junctions. Further testing revealed that the conductance of the molecular junctions using thiol as an anchoring group did not exhibit bias dependence, see ESI Fig. S9.† These results confirm that the bias-dependent molecular conductance is strongly affected by the terminal anchoring groups of the molecules. Notably, minor peaks, as marked by the star symbol, can also be observed in the conductance histogram for NH_2[2] molecular junctions, see Fig. 2e. We attribute the small peak to the NH_2[2] dimer formation *via* an intermolecular hydrogen

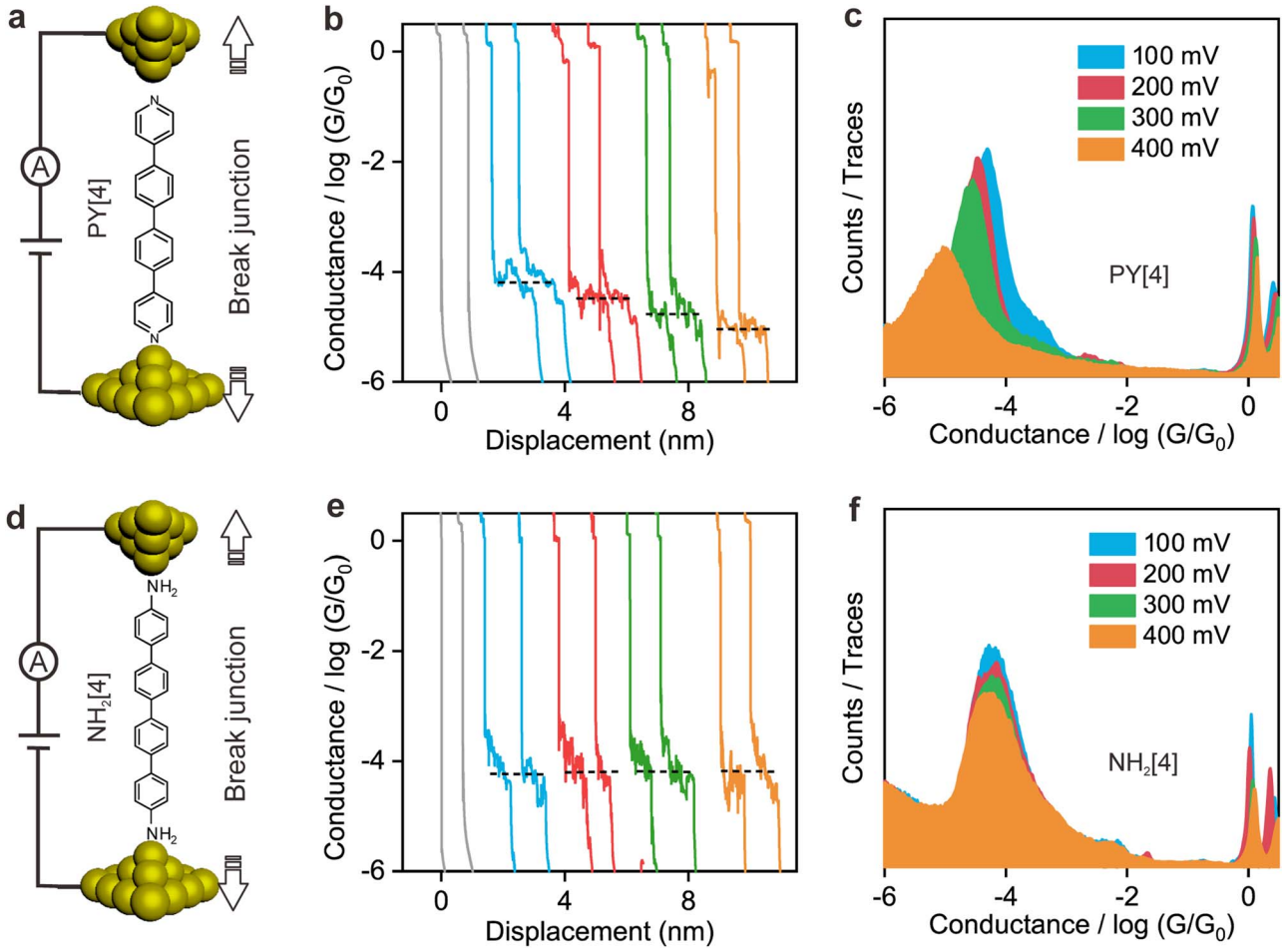

Fig. 1 Conductance of two types of single-molecule dynamic break junctions under different bias voltages. (a) Schematics of a PY[4] molecular break junction where the molecule is bound to the electrode *via* the pyridine–gold link. (b) Typical conductance–displacement traces of bare gold (gray), and PY[4] molecular junctions at bias voltages of 100 mV (blue), 200 mV (red), 300 mV (green), and 400 mV (orange). (c) 1D conductance histograms for PY[4] molecular junctions. (d) Schematics of an NH_2[4] molecular break junction formed *via* an amino–gold link. (e) Typical conductance–displacement traces of bare gold (gray), and NH_2[4] molecular junctions at bias voltages of 100 mV (blue), 200 mV (red), 300 mV (green), and 400 mV (orange). (f) 1D conductance histograms of NH_2[4] molecular junctions under different bias voltages.

bond.[9,33] The individual chemical structures of the molecules and the corresponding conductance under positive bias are summarized in Table 1. Accordingly, the probable conductances of different types of molecular junctions under negative bias are summarized in ESI Table S1.†

More intuitive analysis was carried out to investigate the bias voltage influence on the conductance of the molecules with different anchoring groups. Fig. 2c demonstrates a negative correlation between the conductance of pyridine-anchored molecules and the applied bias voltage, that is, the conductance of molecular junction drops as the absolute magnitude of the bias voltage increases. In contrast, the conductance of the amino-anchored molecules remains relatively constant, and is almost independent of the bias voltage, as shown in Fig. 2f. As an initial conjecture, the distinct behavior of these two types of molecules originates from either the energy structural changes as the molecule is exposed to an external electric field[34,35] or the distinguished conformational changes (*e.g.*, rotation of aromatic rings) regulated by the bias voltage.[13] However, this speculation was ruled out by *I*–*V* measurements of the fixed molecular junctions, which demonstrates that the two types of molecular junctions exhibit the same behavior upon voltage sweeping, as shown below.

Conductance of static fixed molecular junctions

To elucidate the underlying mechanism for the distinct behavior of two types of molecules, we performed *I*–*V* measurement based on the fixed molecular junctions. To perform the *I*–*V* measurement, the movement of the top electrode was paused automatically *via* a feedback system and the molecular junction was allowed to remain fixed for a while (referred to as the electrode-suspension time) once a molecule-bridged junction was formed, which can be judged by the detected conductance. Subsequently, the voltage sweeping mode was triggered, and the corresponding *I*–*V* curves were recorded and used to plot the *I*–*V* density image, see ESI Fig. S10† for detailed information.

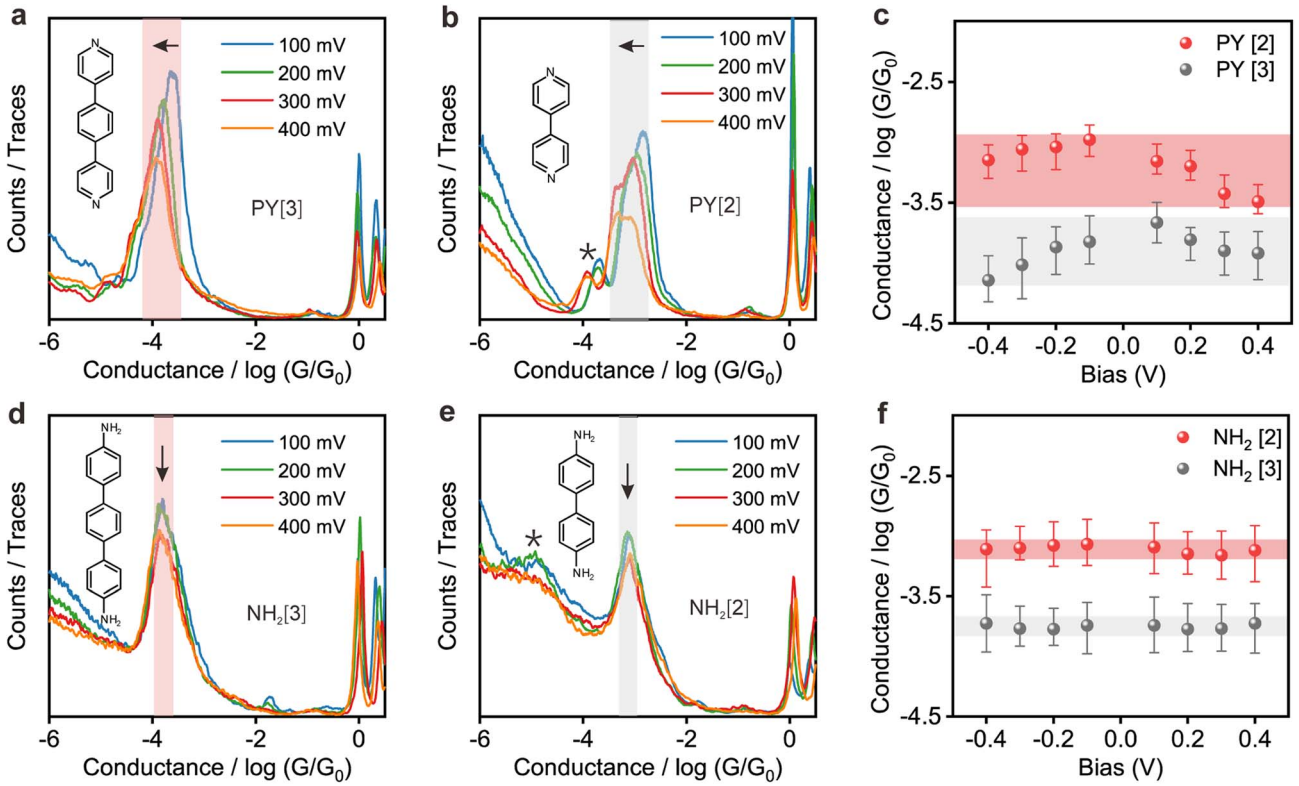

Fig. 2 Conductance histograms of two series of single-molecule break junctions with either amino or pyridyl anchoring groups under different bias voltages. (a) and (b) 1D conductance histograms of PY[3] and PY[2] molecular junctions at different bias voltages. The shaded area highlights the main peaks, which left-shift to a low conductance position as the bias voltage increases. (c) Conductance–voltage plot of pyridine-anchored molecular junctions. The conductance of both PY[3] and PY[2] molecular junction determined by the conductance histogram decreases as the absolute value of bias voltage increases. (d) and (e) 1D conductance histograms of NH_2[3] and NH_2[2] molecular junctions at different bias voltages. The position of the main peaks remains unchanged as the bias voltage increases. (f) Conductance–voltage plot of amino-anchored molecular junctions. The conductance of both NH_2[3] and NH_2[2] molecular junction almost remains unchanged as the absolute value of bias voltage increases. The width of the shaded area indicates the amplitude of the molecular junction conductance variation.

Fig. 3a and b illustrate the 2D logarithmic *I–V* and conductance–voltage (*G–V*) density plotting, which was constructed from approximately 3000 individual *I–V* curves of PY[3] molecular junctions. In contrast to earlier findings shown in dynamic break junctions (Fig. 2c), the *G–V* plot shows that the conductance increases with an increasing bias voltage (Fig. 3b), and Fig. 3c shows the schematic of the fixed PY[3] molecular junctions. For comparison, we also plotted the *I–V* and *G–V* density images of NH_2[3] molecular junctions, as shown in Fig. 3d–f. It is evident that NH_2[3] molecular junctions displayed

Table 1 Molecular structures and corresponding probable conductance determined by 1D conductance histograms under positive bias voltages

		Probable conductance (G_0)			
Molecule	Structure	@100 mV	@200 mV	@300 mV	@400 mV
PY[4]	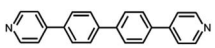	4.53×10^{-5}	3.27×10^{-5}	2.60×10^{-5}	8.58×10^{-6}
PY[3]	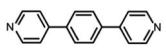	1.37×10^{-4}	9.90×10^{-5}	8.54×10^{-5}	6.82×10^{-5}
PY[2]	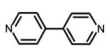	6.95×10^{-4}	6.31×10^{-4}	3.75×10^{-4}	3.22×10^{-4}
NH_2[4]	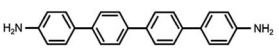	4.61×10^{-5}	5.70×10^{-5}	5.68×10^{-5}	4.87×10^{-5}
NH_2[3]	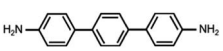	1.82×10^{-4}	1.69×10^{-4}	1.71×10^{-4}	1.88×10^{-4}
NH_2[2]	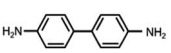	8.06×10^{-4}	7.12×10^{-4}	6.93×10^{-4}	7.60×10^{-4}

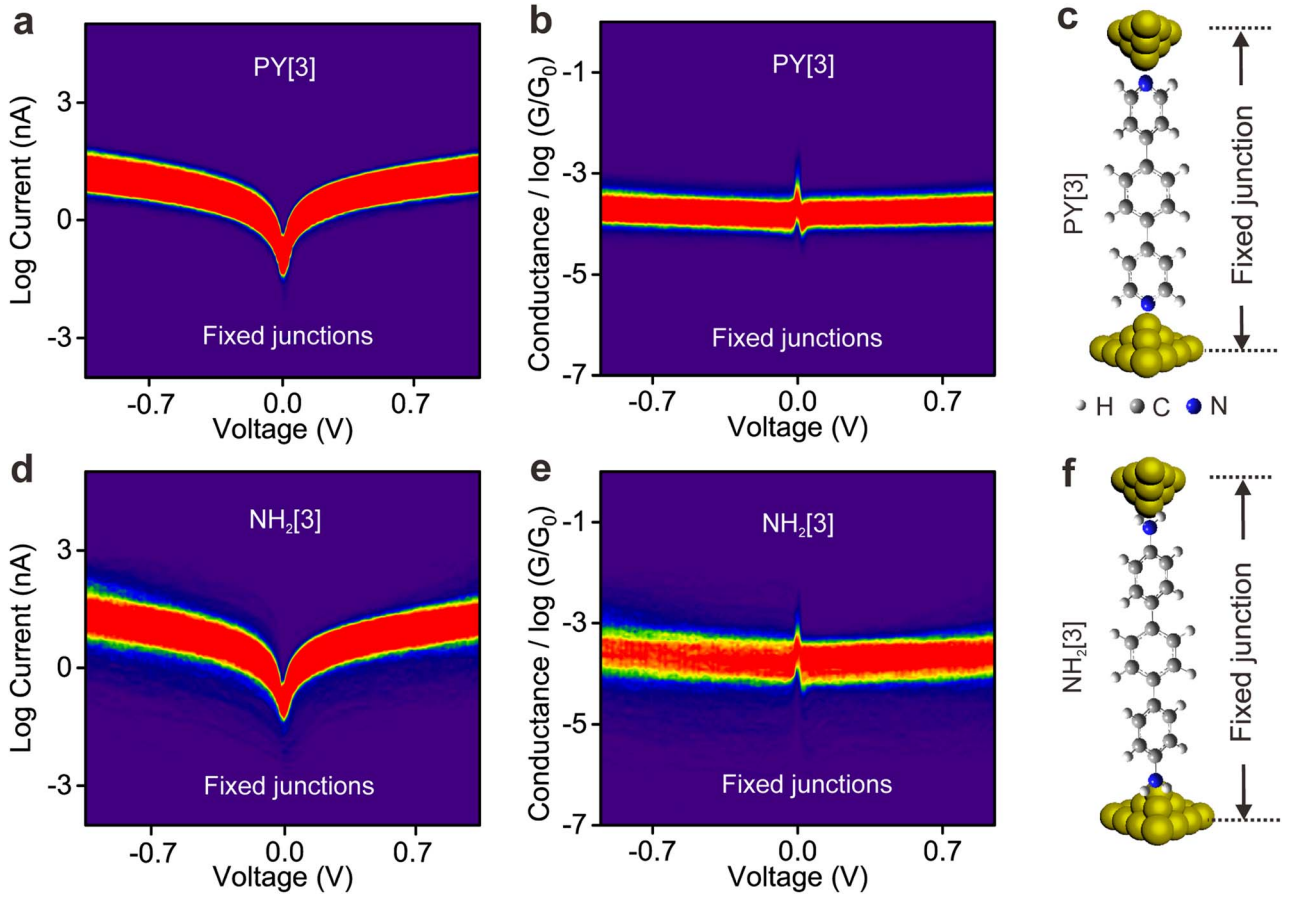

Fig. 3 Density plots of *I*–*V* and *G*–*V* for PY[3] and NH_2[3] single-molecule junctions. (a) 2D density map of *I*–*V* and (b) *G*–*V* curves for PY[3] molecular junctions. Approximately 3200 *I*–*V* curves were used for each plot. (c) Schematic of the PY[3] fixed junction with pyridine-anchoring groups at two ends. The electrode is suspended and the distance between two electrodes is fixed during the *I*–*V* sweeping process. (d) 2D density plot of *I*–*V* and (e) *G*–*V* for NH_2[3] molecular junctions. (f) Schematic of the NH_2[3] fixed junction with amino-anchoring groups at two ends.

an increased conductance with increasing bias voltage as in the case of PY[3]. Additional *I*–*V* measurement shows that the conductance of molecular fixed junctions for NH_2[2] and NH_2[4] also increases upon an increased bias voltage. This behavior is anticipated because the electrode's Fermi level typically approaches the molecular orbital (HOMO or LUMO) when a higher bias voltage is applied, leading to a lower energy barrier and higher conductance,[34,36] see ESI Fig. S11.†

The interesting observation is that the conductance of the pyridine-terminated molecular break junction decreased with increasing applied bias voltage, but the conductance of static fixed junction shows the opposite trend. Notably, the molecule will be exposed to a similar electric field in both break junctions and fixed junctions as the same bias is applied, indicating that the distinct behaviors observed in the two types of junctions do not solely originate from the applied bias voltage. Also, the opposite behavior displayed by two types of junctions effectively eliminates the possibility that the rotation of aromatic ring modulated by the electric field results in conductance changes. Instead, we hypothesize that the distinct behavior of break junctions and fixed junctions originates from the properties of the anchoring group that are strongly influenced by the synergistic action of the electric field and mechanical forces.

Bias dependence of flicker noise spectroscopy

The ability to differentiate between through-space or through-bond electron transport pathways using the flicker noise spectrum has been established.[37,38] In particular, noise power scaling as G^N ($N = 2.0$) refers to electron transport through space while noise power scaling as $G^{1.0}$ corresponds to the through-bond. Here, G represents the average conductance of each junction. Meanwhile, the electron transport channel significantly correlated with the contact geometry,[37,38] and thus the flicker noise spectrum can be used to judge the molecule bonding geometry. The flicker noise measurements were then performed on two different kinds of molecular junctions, see ESI Fig. S12† for further information. Fig. 4a and b show 2D histograms of the normalized noise power plotted against the average conductance of PY[4] molecular junctions. The noise power scales as $G^{1.73}$ at a bias voltage of 100 mV (Fig. 4a) and scales as $G^{1.44}$ at 400 mV (Fig. 4b), which indicates that electron transport through a bond predominates over that through space

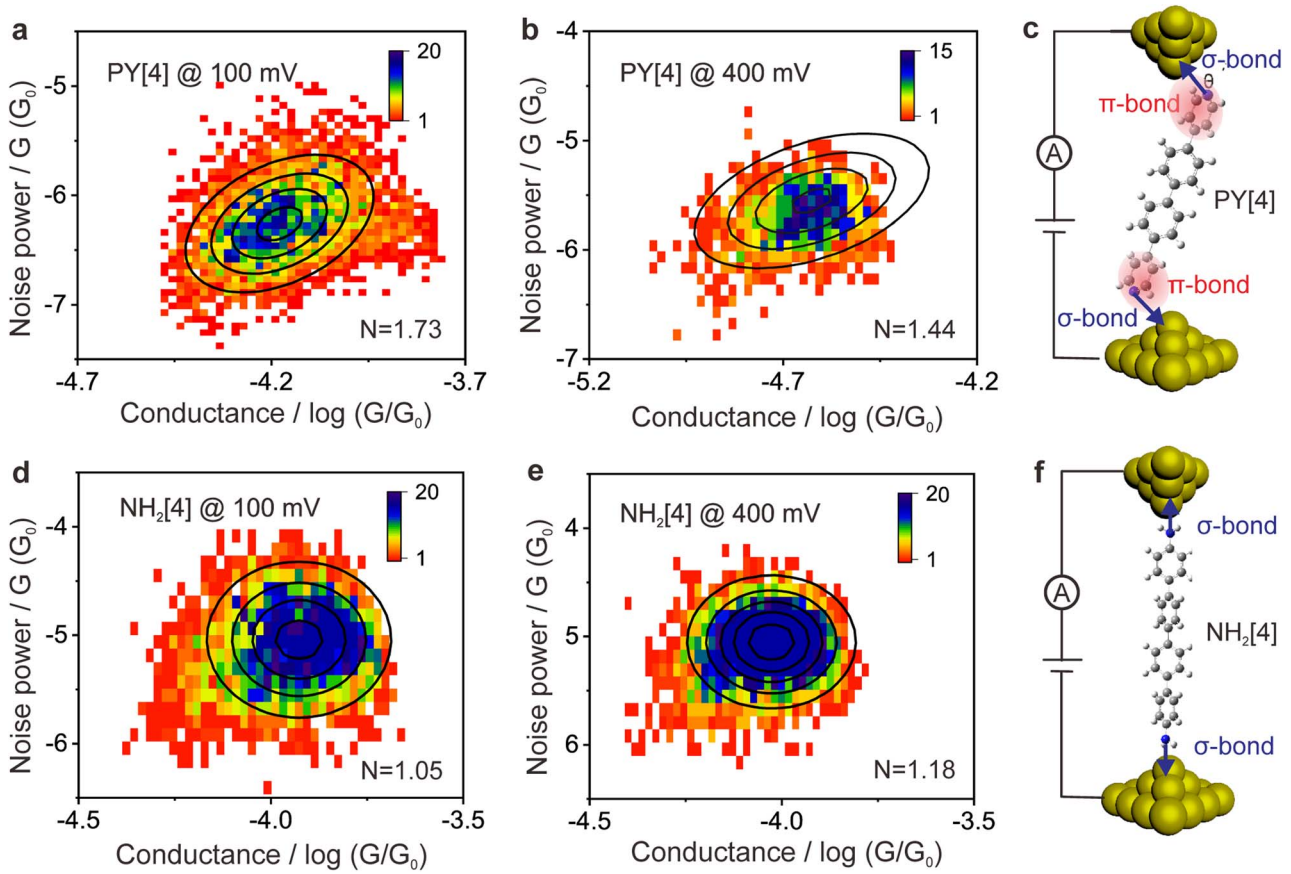

Fig. 4 Flicker noise characterization of the PY[4] and NH_2[4] molecular junctions at different bias voltages. (a) 2D histogram of flicker noise power normalized by G against the average conductance of the junction at 100 mV for PY[4] molecular junctions. (b) 2D histogram of flicker noise power at 400 mV for PY[4] molecular junctions. (c) Diagram of the bonding configurations of the PY[4] molecular junction. The pyridine-anchoring group can couple with the gold electrode through both the σ bond *via* its N atom (indicated by the blue arrow) and the π-bond *via* its aromatic ring (highlighted by the pink shade). (d) Flicker noise characterization of the NH_2[4] molecular junctions at 100 mV and (e) at 400 mV. (f) Diagram of the bonding configurations of the NH_2[4] molecular junction. The amino-anchoring group couples with the gold electrode mainly through the σ bond of its N atom. Each of the noise histograms was established based on approximately 20 000 conductance–time traces and correspondingly a discrete Fourier transform.

in PY[4] molecular junctions under a higher bias voltage. In contrast, the noise power scales as $G^{1.05}$ at a bias voltage of 100 mV and almost retains the same at a bias voltage of 400 mV for NH_2[4] molecular junctions (Fig. 4d and e). The exponent remains unchanged ($N \approx 1$) at both low and high voltages, indicating that the electron transport channel is almost unchanged, *i.e.*, the electrons mainly transport through a bond for NH_2[4] molecular break junctions at both low and high bias voltages.

For pyridine-anchored molecules, the pyridyl can couple with a gold electrode through both the σ bond of its N atom (nitrogen–gold, σ-binding) and the π-bond of its pyridine ring (π-binding),[27,39–41] as schematically shown in Fig. 4c. For the π-binding configuration, the electron is mainly transported through space between the pyridine ring and electrode, which can be seen as a weak coupling compared to the one of σ bond.[26,27] The electronic coupling between the molecular π*-electron and the gold d-electrons decreases as θ (the angle between the nitrogen–gold bond and the plane of the pyridine ring) decreases.[42] The π-coupling is particularly strongest when the nitrogen–gold bond is perpendicular to the pyridine ring (*i.e.*, the angle $\theta = 90°$), and π-coupling is weakest when it is parallel to the pyridine plane (*i.e.*, $\theta = 0°$). The decrease of noise power (N) upon a higher bias voltage (Fig. 4a and b) indicates that the electron transport channel through space (π-coupling) is suppressed. In other words, the decrease of noise power indicates that the nitrogen–gold bond gradually aligns parallel to the direction of the pyridine plane (the same as that of the electric field) upon a higher bias in the dynamical break junctions.

In contrast, for the NH_2[4] molecular junction, the donor–acceptor bond (σ-binding) is primarily formed between the electrode and the anchoring group,[42,43] as schematically presented in Fig. 4f. Due to the lack of π-binding, the electron will primarily be transported through a bond, which results in $N \approx 1$ and it remains unaltered upon a higher bias, as presented in Fig. 4d and e. The absence of π-coupling in NH_2[4] molecular junctions can be attributed to two possible factors: (1) compared to PY[4], the aromatic ring in NH_2[4] is far away from the electrodes by a C–N distance and thus the π-binding

between the aromatic ring and the electrode is relatively weak;[27] (2) the amine–gold link is naturally parallel to the plane of the pyridine ring,[44] and this configuration makes the aromatic ring distant from the electrode and causes a weak π-coupling for the NH_2[4] molecular junction.

Flicker noise spectrum of the PY[2] molecular junction at a low conductance plateau was also carried out, as we mentioned previously. The 2D histogram of the normalized noise power *versus* the average conductance of the molecular junction is displayed in ESI Fig. S13.† It can be found that $N = 1.95$, which indicates that the electron is transported across space rather than through a bond at this state. Combining the observation that the probable low conductance is one order of magnitude smaller than the probable high conductance (Fig. 2b) and the feature of the 2D conductance histogram (Fig. S7†), we believe that the minor peak with low conductance results from the PY [2] dimer formation *via* π–π stacking rather than a single PY[2] molecule with a perpendicular bonding configuration at the interface.

Theoretical calculation

To confirm the proposed mechanism, the transmission of the molecular junctions with different tilt angles was computed based on density functional theory combined with non-equilibrium Green's function. Fig. 5a shows the schematic of molecular junctions with varied tilt angles between the nitrogen–gold bond and pyridine plane, and the correspondingly computed transmission spectra are shown in Fig. 5b. It reveals that the lowest unoccupied molecular π*-orbital (LUMO) is close to the Fermi energy level (E_F), indicating that the LUMO predominantly contributes to the conductance of the PY[4] molecular junction. Fig. 5b demonstrates that the transmission peak broadens as the tilt angle (θ) increases. This feature signifies that the strength of the electronic coupling between the gold electrode and the molecular π*-orbital is enhanced when the nitrogen–gold bond tilts out of the pyridine plane, which supports our conjecture, *i.e.*, change in the orientation of the nitrogen–gold bond will result in the alternation of molecular junction conductance.

Moreover, we can find that the whole transmission coefficient decreases as the tilt angle decreases from 45° to 0°, which indicates that the conductance of the junction will decrease as the orientation of the nitrogen–gold bond changes from being out of the pyridine plane ($\theta = 45°$) to being parallel to the pyridine plane ($\theta = 0°$). This finding is in line with the calculated results of the electron transport pathway, which demonstrates that the volumes of electron transport through the nitrogen–gold bonds decrease when the tilt angle decreases, see ESI Fig. S14.† Transmission eigenstates at 0.3 eV for the PY[4] molecular junction at the tilt angle of 45° and 0° are shown in Fig. 5c and d. It is evident that the spatial distributions of transmission eigenstates at the interface become localized when the tilt angle changes from 45° to 0°, which will result in

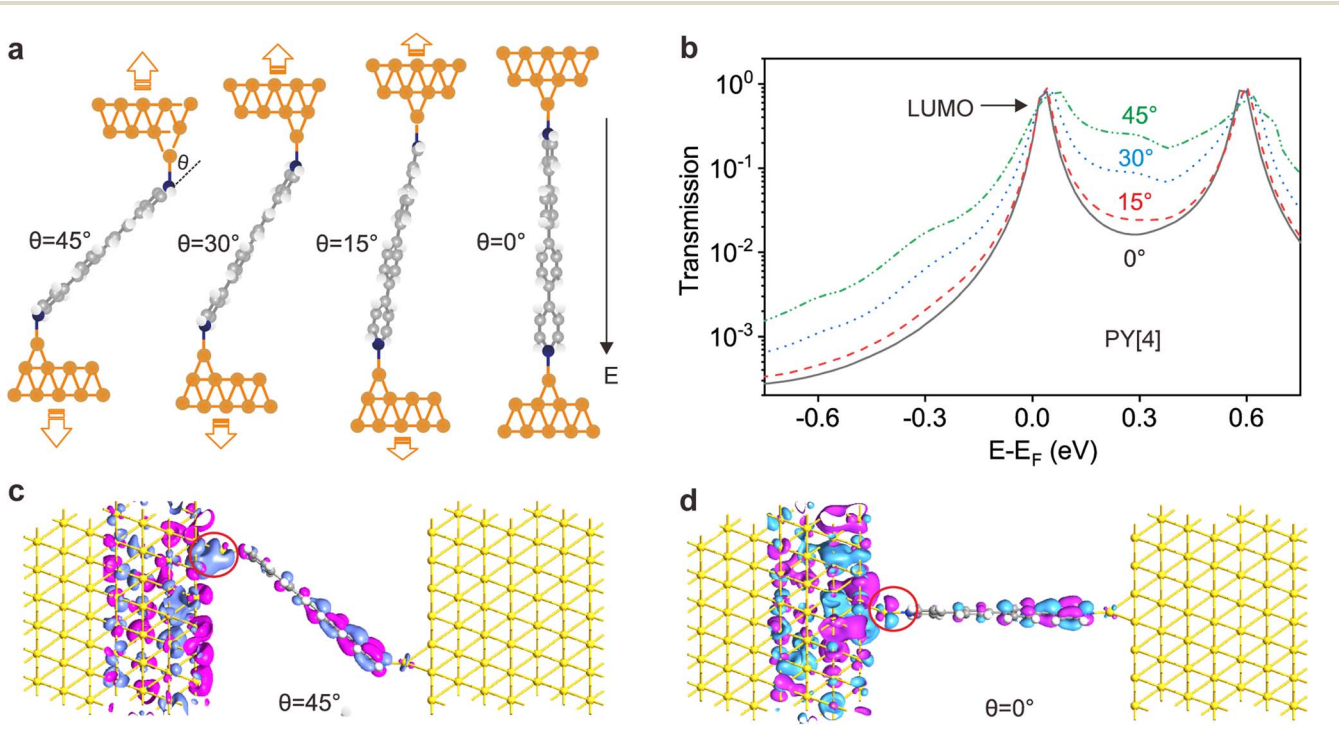

Fig. 5 Transmission characteristics of PY[4] molecular junction with different tilt angles between the nitrogen–gold bond and the pyridine plane (π*-system). (a) Examples of junction geometries relaxed at different tip–sample distances with different nitrogen nitrogen–gold bond orientations. (b) Transmission characteristics plotted on the semi-logarithmic scale for the molecular junctions. The green dotted, blue dashed, red dashed and black solid lines denote the angle (θ) between the nitrogen–gold bond and π*-system, which are 45°, 30°, 15° and 0°, respectively. (c) Transmission eigenstates at 0.3 eV of the PY[4] molecular junction with a tilt angle of 45° and (d) 0°. The red circle highlights the transmission eigenstates at the interface.

a decreased conductance. In contrast, for the NH_2[4] molecular junction, both HOMO and LUMO are far from the Fermi level of the electrode and the wave function at the Fermi level is insensitive to the tilt angle of the molecule compared to PY[4], see ESI Fig. S15.†

We further calculated the electrostatic potential distribution of the molecules with different anchoring groups, see ESI Fig. S16.† It shows that the electrostatic potential around the amino group is positively charged, while the nitrogen atom of the pyridyl group is negatively charged. When the molecule comes in contact with the electrode, a coordination bond will be formed between the anchoring group and the electrode. Under a fixed electric field, the direction of the force undertaken by the amino group and the pyridyl group should be opposite. In that case the external field exerts a pushing force on the pyridyl-based bond (N–Au) and makes the bond tilt angle θ decrease (N–Au gradually parallel to the pyridyl plane) with the assistance of mechanical stretching; the amino-based bond will not experience such a pushing force and thus will not promote the decrease of θ. The change of bond tilt angle will lead to the pronounced variation of the molecular junction conductance, as demonstrated in Fig. 5 in the main text. Thus, the different behaviors of amino-terminated and pyridyl-terminated molecule junctions under the joint action of the electric field and mechanical stretching can also be explained by the distribution of electrostatic potential.

Therefore, the theoretical model calculations, electrostatic potential calculations as well as the measured noise spectra strongly support our hypothesis that the pronounced conductance change of the pyridine-anchored molecular junction highly likely results from the orientation change of the nitrogen–gold bond. With the assistance of mechanical stretching, the orientation of the nitrogen–gold bond gradually aligns with the direction of the increasing electric field. This is anticipated because the nitrogen–gold bond is a coordinate bond, where the electrons for the bond formation are solely supplied by the N atom (so-called semi-polar bond) and is highly sensitive to the direction of the external electric field.[21] This bond orientation change reduces the coupling strength by suppressing the π coupling channel between the pyridine ring and electrode. The orientation change of the nitrogen–gold bonds with increasing bias not only makes the molecular coupling strength weaker in line with the decreased conductance, but also gives rise to the following features: (1) the length of the conductance plateau decreases, since a weak coupling facilitates the breakage of the junction and thus makes the lifetime of the junction short, which agrees well with the experimental observation as presented in ESI Fig. S2–S7;† and (2) the intensity of the peak in the conductance histogram decreases due to the decreased lifetime of the junction and decreased length of the conductance plateau, which is consistent with the feature seen in Fig. 1c and 2a, b.

We would like to emphasize that (1) the electric field activation alone does not result in a change in the orientation of the nitrogen–gold bond. This claim is supported by the *I–V* test, which shows that in a static fixed junction, the conductance decrease is not observed when the electric field is increased during the voltage sweeping process (Fig. 3); (2) the sole activation of mechanical stretching cannot trigger the change of nitrogen–gold orientation in a pyridyl-anchored molecular junction either. If mechanical stretching alone has the capability to alter the nitrogen–gold orientation, the conductance of the junction would no longer depend on the bias voltage; (3) only the synergistic action of dynamical mechanical stretching and electric field activation can regulate the orientation of the pyridine–gold link in the coordinate bond terminated molecular break junction.

As a discussion, although the conductance of the molecular junctions using thiol and amino as anchoring groups does not exhibit bias dependence, we cannot draw the conclusion that the orientation of the S–Au or amino–Au bond can't be modulated by the synergistic action of mechanical forces and electric field, because the π-coupling was absent in these molecular junctions and the orientational change of the S–Au/N–Au bond might not result in a notable conductance variation. Our additional calculations show that the binding energies of PY[4] and NH_2[4] on the electrode surface are approximately 1.604 eV and 0.509 eV, respectively. The diverse binding energy may result in different behaviors of amino and pyridyl-anchored molecular junctions as well. For the amino-anchored molecular junction with weak bonding strength, the orientation of the N–Au bond may be modulated by the sole mechanical stretching already, resulting in the observation that the conductance does not depend on the bias voltage any more. To address whether it is feasible to regulate the orientation of amino–Au and S–Au bond by the same strategy, additional experiments are highly desired.

Conclusion

In summary, we investigated the influence of electric field strength and mechanical stretching on the bonding orientation of two types of molecular junctions: dynamic break junctions and static fixed junctions. Employing the single-molecule break junction technique, we observed a decrease in the conductance of pyridine-anchored molecular junctions as the bias voltage increases. In contrast, the conductance of the static fixed molecular junctions with identical molecules increases as the bias voltage increases by utilizing the electrode suspension function of the device. This opposite behavior in the two types of junctions indicates that the conductance of the junction is modulated by the synergistic interplay of mechanical stretching and electric field. With the assistance of flicker noise spectra measurements and DFT-based calculations, we revealed that the electric field, coupled with the mechanical stretching, can regulate the orientation of the pyridine–gold bond to align with the direction of the increased electric field which reduces the coupling strength between the pyridine π*-system and electrode, ultimately resulting in a pronounced decrease in conductance. In contrast, this phenomenon was not observed in amino-anchored and thiol-anchored molecular junctions due to the absence of π-coupling. Our study provides a framework for characterizing and regulating the orientation of a single chemical bond in single molecular junctions. This approach shows promise for achieving precise control over the behavior

of single molecules, facilitating the modulation of electron transport across single-molecule junctions and opening up a path to the realization of molecular functional devices.

Data availability

Further details of the experimental procedure, fabrication of the STM tip and substrate, conductance of single-molecule break junctions under different biases, *I–V* measurement of fixed molecular junctions, flicker noise power spectroscopy, DFT calculation of electron transport through molecular junctions and molecular electrostatic potential distribution are available in the ESI.†

Author contributions

D. X., initiated the project. W. Z., performed electrical measurement and carried out the electrostatic potential calculation. Z. Z., performed AFM measurement. Z. F., performed DFT calculations. W. Z. and D. X., wrote the manuscript with contributions from all authors.

Conflicts of interest

The authors declare no competing financial interests.

Acknowledgements

We acknowledge the financial support from the National Key R&D Program of China (2021YFA1200103), the National Natural Science Foundation of China (22273041, 91950116, 11804170), and the Natural Science Foundation of Tianjin (19JCZDJC31000, 19JCJQJC60900, 22JCYBJC01310).

Notes and references

1 S. V. Aradhya and L. Venkataraman, Single-molecule junctions beyond electronic transport, *Nat. Nanotechnol.*, 2013, **8**, 399–410.
2 C. Jia, A. Migliore, N. Xin, S. Huang, J. Wang, Q. Yang, S. Wang, H. Chen, D. Wang, B. Feng, Z. Liu, G. Zhang, D. H. Qu, H. Tian, M. A. Ratner, H. Q. Xu, A. Nitzan and X. Guo, Covalently bonded single-molecule junctions with stable and reversible photoswitched conductivity, *Science*, 2016, **352**, 1443–1445.
3 D. Xiang, X. Wang, C. Jia, T. Lee and X. Guo, Molecular-Scale Electronics: From Concept to Function, *Chem. Rev.*, 2016, **116**, 4318–4440.
4 M. Wang, T. Wang, O. S. Ojambati, T. J. Duffin, K. Kang, T. Lee, E. Scheer, D. Xiang and C. A. Nijhuis, Plasmonic phenomena in molecular junctions: principles and applications, *Nat. Rev. Chem.*, 2022, **6**, 681–704.
5 M. L. Perrin, E. Burzurí and H. S. van der Zant, Single-molecule transistors, *Chem. Soc. Rev.*, 2015, **44**, 902–919.
6 D. Xiang, H. Jeong, D. Kim, T. Lee, Y. Cheng, Q. Wang and D. Mayer, Three-Terminal Single-Molecule Junctions Formed by Mechanically Controllable Break Junctions with Side Gating, *Nano Lett.*, 2013, **13**, 2809–2813.
7 L. Chen, A. Feng, M. Wang, J. Liu, W. Hong, X. Guo and D. Xiang, Towards single-molecule optoelectronic devices, *Sci. China: Chem.*, 2018, **61**, 1368–1384.
8 A. Giguère, M. Ernzerhof and D. Mayou, Surface Plasmon Polariton-Controlled Molecular Switch, *J. Phys. Chem. C*, 2018, **122**, 20083–20089.
9 Z. Zhao, C. Guo, L. Ni, X. Zhao, S. Zhang and D. Xiang, In situ photoconductivity measurements of imidazole in optical fiber break-junctions, *Nanoscale Horiz.*, 2021, **6**, 386–392.
10 C. Bruot, J. Hihath and N. Tao, Mechanically controlled molecular orbital alignment in single molecule junctions, *Nat. Nanotechnol.*, 2012, **7**, 35–40.
11 I. Franco, C. B. George, G. C. Solomon, G. C. Schatz and M. A. Ratner, Mechanically Activated Molecular Switch through Single-Molecule Pulling, *J. Am. Chem. Soc.*, 2011, **133**, 2242–2249.
12 M. Kamenetska, J. R. Widawsky, M. Dell'Angela, M. Frei and L. Venkataraman, Temperature dependent tunneling conductance of single molecule junctions, *J. Chem. Phys.*, 2017, **146**, 092311.
13 W. Lee, S. Louie, A. M. Evans, N. M. Orchanian, I. B. Stone, B. Zhang, Y. Wei, X. Roy, C. Nuckolls and L. Venkataraman, Increased Molecular Conductance in Oligo[n]phenylene Wires by Thermally Enhanced Dihedral Planarization, *Nano Lett.*, 2022, **22**, 4919–4924.
14 D. Miura, K. Iwata, S. Kurokawa and A. Sakai, Break Voltage of the $1G_0$ Contact of Noble Metals and Alloys, *e-J. Surf. Sci. Nanotechnol.*, 2009, **7**, 891–897.
15 H. Song, M. A. Reed and T. Lee, Single Molecule Electronic Devices, *Adv. Mater.*, 2011, **23**, 1583–1608.
16 P. Liljeroth, J. Repp and G. A. Meyer, Current-Induced Hydrogen Tautomerization and Conductance Switching of Naphthalocyanine Molecules, *Science*, 2007, **317**, 1203–1206.
17 S. Shaik, D. Mandal and R. Ramanan, Oriented electric fields as future smart reagents in chemistry, *Nat. Chem.*, 2016, **8**, 1091–1098.
18 A. Zhang, X. Zhuang, J. Liu, J. Huang, L. Lin, Y. Tang, S. Zhao, R. Li, B. Wang, B. Fang and W. Hong, Catalytic cycle of formate dehydrogenase captured by single-molecule conductance, *Nat. Catal.*, 2023, **6**, 266–275.
19 S. Shaik, D. Danovich, J. Joy, Z. Wang and T. Stuyver, Electric-Field Mediated Chemistry: Uncovering and Exploiting the Potential of (Oriented) Electric Fields to Exert Chemical Catalysis and Reaction Control, *J. Am. Chem. Soc.*, 2020, **142**, 12551–12562.
20 H. Li, T. A. Su, V. Zhang, M. L. Steigerwald, C. Nuckolls and L. Venkataraman, Electric field breakdown in single molecule junctions, *J. Am. Chem. Soc.*, 2015, **137**, 5028–5033.
21 M. Omidian, S. Leitherer, N. Néel, M. Brandbyge and J. Kröger, Electric-Field Control of a Single-Atom Polar Bond, *Phys. Rev. Lett.*, 2021, **126**, 216801.
22 J. Lin, Y. Lv, K. Song, X. Song, H. Zang, P. Du, Y. Zang and D. Zhu, Cleavage of non-polar $C(sp^2)$–$C(sp^2)$ bonds in cycloparaphenylenes via electric field-catalyzed

electrophilic aromatic substitution, *Nat. Commun.*, 2023, **14**, 293.

23 B. Zhang, C. Schaack, C. R. Prindle, E. A. Vo, M. Aziz, M. L. Steigerwald, T. C. Berkelbach, C. Nuckolls and L. Venkataraman, Electric fields drive bond homolysis, *Chem. Sci.*, 2023, **14**, 1769–1774.

24 G. Mezei, Z. Balogh, A. Magyarkuti and A. Halbritter, Voltage-Controlled Binary Conductance Switching in Gold-4,4′-Bipyridine-Gold Single-Molecule Nanowires, *J. Phys. Chem. Lett.*, 2020, **11**, 8053–8059.

25 L. Tučková, A. Jaroš, C. Foroutan-Nejad and M. Straka, A quest for ideal electric field-driven MX@C70 endohedral fullerene memristors: which MX fits the best?, *Phys. Chem. Chem. Phys.*, 2023, **25**, 14245–14256.

26 Y. Wei, L. Li, J. E. Greenwald and L. Venkataraman, Voltage-Modulated van der Waals Interaction in Single-Molecule Junctions, *Nano Lett.*, 2023, **23**, 567–572.

27 Z. Yu, Y.-X. Xu, J.-Q. Su, P. M. Radjenovic, Y.-H. Wang, J.-F. Zheng, B. Teng, Y. Shao, X.-S. Zhou and J.-F. Li, Probing Interfacial Electronic Effects on Single-Molecule Adsorption Geometry and Electron Transport at Atomically Flat Surfaces, *Angew. Chem., Int. Ed.*, 2021, **60**, 15452–15458.

28 H. Ohnishi, Y. Kondo and K. Takayanagi, Quantized conductance through individual rows of suspended gold atoms, *Nature*, 1998, **395**, 780–783.

29 B. Xu and N. J. Tao, Measurement of single-molecule resistance by repeated formation of molecular junctions, *Science*, 2003, **301**, 1221–1223.

30 Y. Tang, Y. Zhou, D. Zhou, Y. Chen, Z. Xiao, J. Shi, J. Liu and W. Hong, Electric Field-Induced Assembly in Single-Stacking Terphenyl Junctions, *J. Am. Chem. Soc.*, 2020, **142**, 19101–19109.

31 R. Frisenda, V. A. E. C. Janssen, F. C. Grozema, H. S. J. van der Zant and N. Renaud, Mechanically controlled quantum interference in individual π-stacked dimers, *Nat. Chem.*, 2016, **8**, 1099–1104.

32 S. Wu, M. T. González, R. Huber, S. Grunder, M. Mayor, C. Schönenberger and M. Calame, Molecular junctions based on aromatic coupling, *Nat. Nanotechnol.*, 2008, **3**, 569–574.

33 X. Zhao, X. Zhang, K. Yin, S. Zhang, Z. Zhao, M. Tan, X. Xu, Z. Zhao, M. Wang, B. Xu, T. Lee, E. Scheer and D. Xiang, In Situ Adjustable Nanogaps and In-Plane Break Junctions, *Small Methods*, 2023, **7**, 2201427.

34 C. Guo, X. Chen, S.-Y. Ding, D. Mayer, Q. Wang, Z. Zhao, L. Ni, H. Liu, T. Lee and B. Xu, Molecular orbital gating surface-enhanced Raman scattering, *ACS Nano*, 2018, **12**, 11229–11235.

35 S.-X. Li, D.-L. Chen, Z.-P. Zhang, Z.-W. Long and S.-J. Qin, Study on the ground state properties and excitation properties of C18 under different external electric fields, *Acta Phys. Sin.*, 2020, **69**, 103101.

36 Z. Zhao, W. Wang, X. Zhou, L. Ni, K. Kang, T. Lee, H. Han, H. Yuan, C. Guo and M. Wang, Crystal Size Effect on Carrier Transport of Microscale Perovskite Junctions via Soft Contact, *Nano Lett.*, 2020, **20**, 8640–8646.

37 O. Adak, E. Rosenthal, J. Meisner, E. F. Andrade, A. N. Pasupathy, C. Nuckolls, M. S. Hybertsen and L. Venkataraman, Flicker Noise as a Probe of Electronic Interaction at Metal–Single Molecule Interfaces, *Nano Lett.*, 2015, **15**, 4143–4149.

38 J. Li, Z. Zhuang, P. Shen, S. Song, B. Z. Tang and Z. Zhao, Achieving Multiple Quantum-Interfered States via Through-Space and Through-Bond Synergistic Effect in Foldamer-Based Single-Molecule Junctions, *J. Am. Chem. Soc.*, 2022, **144**, 8073–8083.

39 T. Dadosh, Y. Gordin, R. Krahne, I. Khivrich, D. Mahalu, V. Frydman, J. Sperling, A. Yacoby and I. Bar-Joseph, Measurement of the conductance of single conjugated molecules, *Nature*, 2005, **436**, 677–680.

40 C. A. Martin, D. Ding, H. S. J. van der Zant and J. M. v. Ruitenbeek, Lithographic mechanical break junctions for single-molecule measurements in vacuum: possibilities and limitations, *New J. Phys.*, 2008, **10**, 065008.

41 S. T. Schneebeli, M. Kamenetska, Z. Cheng, R. Skouta, R. A. Friesner, L. Venkataraman and R. Breslow, Single-molecule conductance through multiple π-π-stacked benzene rings determined with direct electrode-to-benzene ring connections, *J. Am. Chem. Soc.*, 2011, **133**, 2136–2139.

42 S. Quek, M. Kamenetska, M. Steigerwald, H. Choi, S. Louie, M. Hybertsen, J. Neaton and L. Venkataraman, Mechanically controlled binary conductance switching of a single-molecule junction, *Nat. Nanotechnol.*, 2009, **4**, 230–234.

43 M. S. Hybertsen, L. Venkataraman, J. E. Klare, A. C. Whalley, M. L. Steigerwald and C. Nuckolls, Amine-linked single-molecule circuits: systematic trends across molecular families, *J. Phys.: Condens. Matter*, 2008, **20**, 374115.

44 S. Y. Quek, L. Venkataraman, H. J. Choi, S. G. Louie, M. S. Hybertsen and J. B. Neaton, Amine-gold linked single-molecule circuits: experiment and theory, *Nano Lett.*, 2007, **7**, 3477–3482.